Supplementary Information for:

Influence of Structure on Exchange Strength and Relaxation Barrier in a Series of $FeRe(CN)_2$ Single-Chain Magnets

Xiaowen Feng, T. David Harris, and Jeffrey R. Long*

Department of Chemistry, University of California, Berkeley, California 94720,
E-mail: jrlong@berkeley.edu

Chem. Sci.

Table of Contents

Experimental Section

Preparation of Compounds: The compounds $(Bu_4N)_2$[*trans*-$ReCl_4(CN)_2$]·2DMA and $(DMF)_4FeReCl_4(CN)_2$ (**3**) were synthesized as described previously.[10] Solid $(Bu_4N)CN$ was dried in vacuo ($P < 10^{-3}$ Torr) for 36 h using a trap containing P_2O_5 prior to use. All other reagents were obtained from commercial sources and used without further purification. *Caution!* Although we have experienced no problems while working with them, perchlorate salts are potentially explosive and should be handled with extreme care and only in small quantities.

$(DEF)_4FeReCl_4(CN)_2$ (1). A solution containing $Fe(ClO_4)_2·6H_2O$ (0.020 g, 0.078 mmol) in 2 mL of diethylformamide (DEF) was added to a solution of $(Bu_4N)_2[ReCl_4(CN)_2]$·2DMA (0.030 g, 0.035 mmol) in 2 mL of DEF. The resulting deep blue solution was allowed to stand for 12 h to afford blue plated-shaped crystals, suitable for single-crystal X-ray diffraction. The crystals were collected by filtration, washed with successive aliquots of DEF (3 × 1 mL) and Et_2O (3 × 5 mL), and then were allowed to dry in air to give **1** (0.018 g, 59%) as a dark blue solid. IR: ν_{CN} 2151cm^{-1}. Anal. Calcd for $C_{22}H_{44}Cl_4FeN_6O_4Re$: C, 31.44; H, 5.28; N, 10.00; Found: C, 31.27; H, 5.38; N, 10.32.

$(DBF)_4FeReCl_4(CN)_2$ (2). A solution containing $(Bu_4N)_2[ReCl_4(CN)_2]$·2DMA (0.040 g, 0.038 mmol) in 3 mL of dibutylformamide (DBF) was carefully layered on top of a solution containing $Fe(ClO_4)_2·6H_2O$ (0.020 g, 0.078 mmol) in 3 mL of DBF. Upon standing for two days, dark blue block-shaped crystals, suitable for single-crystal X-ray diffraction, formed from the layering. The crystals were collected by filtration, washed with Et_2O (3 × 2 mL), and dried in air to give **2** (0.012 g, 35%) as a dark blue solid. IR: ν_{CN} 2155 cm^{-1}. Anal. Calcd for $C_{38}H_{76}Cl_4FeN_6O_4Re$: C, 43.93; H, 7.37; N, 8.09; Found: C, 44.25; H, 7.62; N, 8.78.

$(DMB)_4FeReCl_4(CN)_2$ (4). A solution containing $(Bu_4N)_2[ReCl_4(CN)_2]$·2DMA (0.040 g, 0.038 mmol) in 2 mL of dimethylbutyramide (DMB) was carefully layered on top of a solution containing $Fe(ClO_4)_2·6H_2O$ (0.020 g, 0.078 mmol) in 2 mL of DMB. Upon standing for one day, dark blue plate-shaped crystals, suitable for single-crystal X-ray diffraction, formed from the layering. The crystals were collected by filtration, washed with Et_2O (3 × 2 mL), and dried in air to give **4** (0.010 g, 29%) as a dark blue solid. IR: ν_{CN} 2158 cm^{-1}. Anal.

Calcd for $C_{26}H_{52}Cl_4FeN_6O_4Re$: C, 34.83 H, 5.85; N, 9.38; Found: C, 34.65; H, 5.55; N, 9.25.

$(DMP)_4FeReCl_4(CN)_2$ (5). A solution containing $(Bu_4N)_2[ReCl_4(CN)_2]\cdot 2DMA$ (0.044 g, 0.042 mmol) in 2 mL of dimethylpropionamide (DMP) was carefully layered on top of a solution containing $Fe(ClO_4)_2\cdot 6H_2O$ (0.014 g, 0.055 mmol) in 2 mL of DMP. Upon standing for one day, dark blue plate-shaped crystals, suitable for single-crystal X-ray diffraction, formed from the layering. The crystals were collected by filtration, washed with Et_2O (3 × 2 mL), and dried in air to give **4** (0.011 g, 33%) as a dark blue solid. IR: ν_{CN} 2160 cm^{-1}, Anal. Calcd for $C_{22}H_{44}Cl_4FeN_6O_4Re$: C, 33.67 H, 5.65; N, 10.71; Found: C, 33.65; H, 5.78; N, 10.82.

$(DEA)_4FeReCl_4(CN)_2$ (6). A solution containing $(Bu_4N)_2[ReCl_4(CN)_2]\cdot 2DMA$ (0.040 g, 0.038 mmol) in 3 mL of diethylacetamide (DEA) was carefully layered on top of a solution containing $Fe(ClO_4)_2\cdot 6H_2O$ (0.027 g, 0.11 mmol) in 3 mL of DEA. Upon standing for 3 days, dark blue block-shaped crystals, suitable for single-crystal X-ray diffraction, formed from the layering. The crystals were collected by filtration, washed with Et_2O (3 × 2 mL), and dried in air to give **4** (0.012 g, 35%) as a dark blue solid. IR: ν_{CN} 2162 cm^{-1}, Anal. Calcd for $C_{32}H_{65}Cl_4FeN_7O_4Re$: C, 31.44; H, 5.28; N, 10.00; Found: C, 31.69; H, 5.24; N, 9.95.

X-Ray Structure Determinations. Single crystals of compounds **1**, **2, 4, 5** and **6** were coated with Paratone-N oil and mounted on glass fibers or Kaptan loops. The crystals were then quickly transferred to a Bruker APEX or Bruker MICROSTAR diffractometer, and cooled in a stream of nitrogen gas. Preliminary cell data were collected, giving unit cells with the triclinic, monoclinic, or tetragonal Laue group for all compounds, using the SMART[1] or APEX2[2] program package. The unit cell parameters were later refined against all data. A full hemisphere of data was collected for all compounds. None of the crystals showed significant decay during data collection. Data were integrated and corrected for Lorentz and polarization effects using SAINT[3] and were corrected for absorption effects using SADABS[4].

Space group assignments were based upon systematic absences, *E*-statistics, and successful refinement of the structures. Structures were solved by direct methods and expanded through successive difference Fourier maps. They were refined against all data using the SHELXTL[5] program. Thermal parameters for all non-hydrogen atoms were refined anisotropically in all

compounds. Table 1 summarizes the unit cell and structure refinement parameters for compounds **1**, **2**, and **4-6**.

Magnetic Susceptibility Measurements. Magnetic data were collected on a Quantum Design MPMS-XL SQUID magnetometer. Dc susceptibility, dc magnetization and ac susceptibility measurements for **6** were obtained for a microcrystalline powder restrained in its frozen mother liquor within a sealed quartz tubes to prevent sample decomposition. All measurements of compounds **1**, **2**, **4** and **5** were obtained for microcrystalline powders restrained in a frozen polyethylene bag. Dc magnetization data were collected at 1.8 K while sweeping the magnetic field between 7 and −7 T. Ac magnetic susceptibility data were collected in zero dc field in the temperature range 1.7-10 K, under an ac field of 4 Oe oscillating at frequencies in the range 0.5-1488 Hz. For compound **4**, ac magnetic susceptibility data were also collected under a dc field of 1000 Oe. All data were corrected for diamagnetic contributions from the sample holder, as well as for the core diamagnetism of each sample (estimated using Pascal's constants).

Other Physical Measurements. Infrared spectra were obtained on a Nicolet Avatar 360 FTIR with an attenuated total reflectance accessory (ATR). Carbon, hydrogen, and nitrogen analyses were obtained from the Microanalytical Laboratory of the University of California, Berkeley. X-ray powder diffraction data were collected using Cu Kα (λ = 1.5406 Å) radiation on a Siemens D5000 diffractometer.

Reference

1. *SMART Software Users Guide*, *Version 5.1*; Bruker Analytical X-Ray Systems: Madison, WI, 1999.
2. APEX2 v.2009; Bruker Analytical, Version 7.0; Bruker Analytical X-Ray System: Madison, WI, 1999.
3. *SAINT Software Users Guide*, Version 7.0; Bruker Analytical X-Ray Systems: Madison, WI, 1999.
4. Sheldrick, G. M. SADABS, Version 2.03; Bruker Analytical X-Ray Systems, Madison, WI, 2000.
5. Sheldrick, G. M. SHELXTL, Version 6.12; Bruker Analytical X-Ray Systems, Madison, WI, 2000.

Table S1. Crystallographic data[a] for $L_4FeReCl_4(CN)_2$ (L = DEF (**1**), DBF (**2**), DMF (**3**), DMB (**4**), DMP (**5**), DEA (**6**)).

	1	**2**	**4**	**5**	**6**
formula	$C_{22}H_{44}Cl_4FeN_6O_4Re$	$C_{38}H_{76}Cl_4FeN_6O_4Re$	$C_{22}H_{44}Cl_4FeN_6O_4Re$	$C_{26}H_{52}Cl_4FeN_6O_4Re$	$C_{32}H_{65}Cl_4FeN_6O_4Re$
fw	840.49	1064.91	840.49	896.60	981.76
T, K	100	100	110	100	149
space group	P 1	$P-1$	$P-1$	P 2/n	P 4/n
Z	1	1	1	2	2
a, Å	8.6226(8)	8.9350(1)	9.4650(15)	10.7780(8)	13.3667(17)
b, Å	10.3074(10)	10.5040(1)	9.9760(15)	12.3160(10)	13.3667(17)
c, Å	10.4929(10)	14.0630(1)	10.6310(13)	14.4070(10)	10.7152(13)
α, deg	104.878(4)	68.984(4)	108.439(8)	90.000(0)	90.000(0)
β, deg	92.699(4)	77.296(4)	109.416(9)	107.013(8)	90.000(0)
γ, deg	101.666(4)	85.408(4)	106.268(8)	90.000(0)	90.000(0)
V, Å^3	877.85(14)	1201.90(10)	810.58(17)	1828.72(14)	1914.47(4)
d_{calc}, g/cm^3	1.592	1.451	1.721	1.635	1.560
R_1 (wR_2), %[b]	2.15 (5.70)	5.45 (14.20)	3.41 (9.32)	5.31 (14.37)	2.91 (7.67)

[a]Obtained with graphite-monochromated Mo Kα (λ = 0.71073 Å) radiation for **2** and **5**, and Cu Kα (λ = 1.5406 Å) for **1**, **4**, and **6**. [b] $R_1 = \Sigma||F_o| - |F_c||/\Sigma|F_o|$, $wR_2 = \{\Sigma\,[w(F_o^2 - F_c^2)^2]\}^{1/2}$.

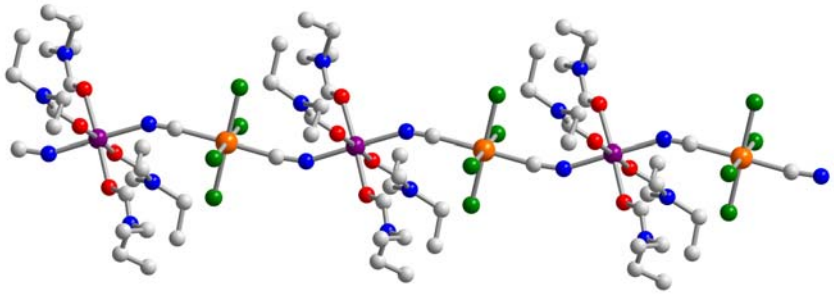

Figure S1. Crystal structure of $(DEF)_4FeReCl_4(CN)_2$ **1** chain. Orange, purple, green, red, blue, and gray spheres represent rhenium, iron, chlorine, oxygen, nitrogen, and carbon atoms, respectively; hydrogen atoms have been omitted for clarity.

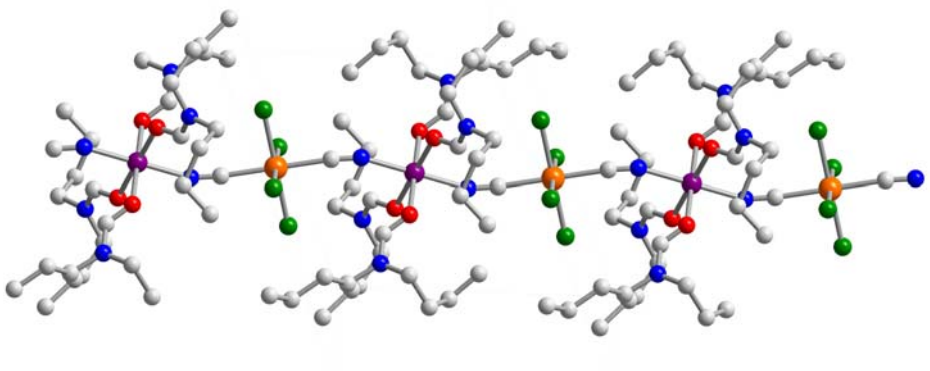

Figure S2. Crystal structure of $(DBF)_4FeReCl_4(CN)_2$ **2** chain. Orange, purple, green, red, blue, and gray spheres represent rhenium, iron, chlorine, oxygen, nitrogen, and carbon atoms, respectively; hydrogen atoms have been omitted for clarity.

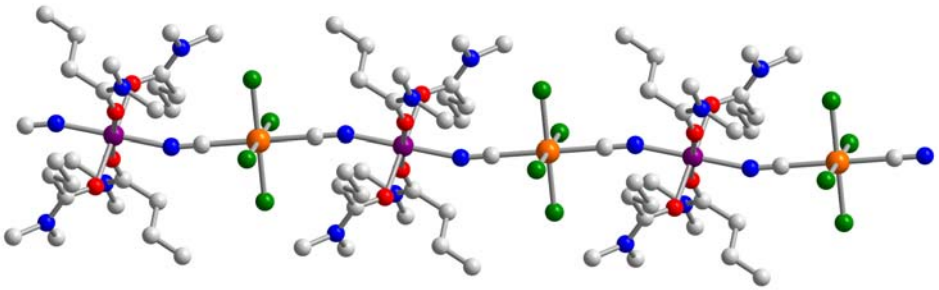

Figure S3. Crystal structure of $(DMB)_4FeReCl_4(CN)_2$ **4** chain. Orange, purple, green, red, blue, and gray spheres represent rhenium, iron, chlorine, oxygen, nitrogen, and carbon atoms, respectively; hydrogen atoms have been omitted for clarity.

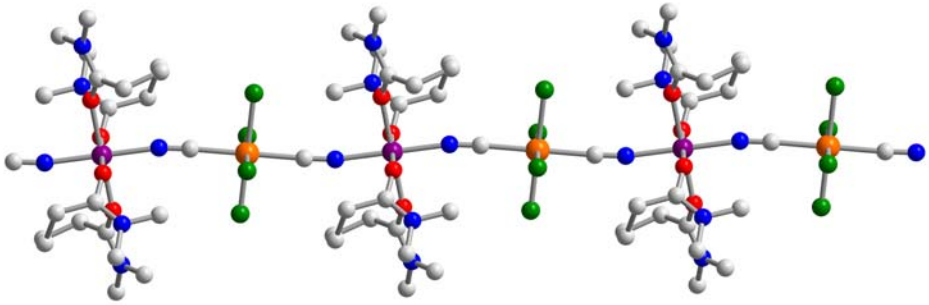

Figure S4. Crystal structure of $(DMP)_4FeReCl_4(CN)_2$ **5** chain. Orange, purple, green, red, blue, and gray spheres represent rhenium, iron, chlorine, oxygen, nitrogen, and carbon atoms, respectively; hydrogen atoms have been omitted for clarity.

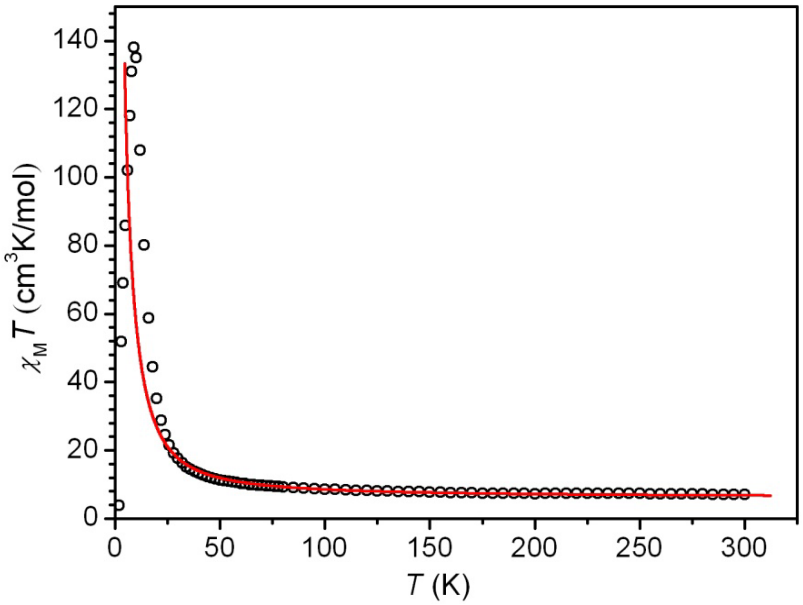

Figure S5. Variable-temperature dc magnetic susceptibility data for **1**, collected in an applied field of 1000 Oe. The solid red line corresponds to a fit to the data, as described in the text.

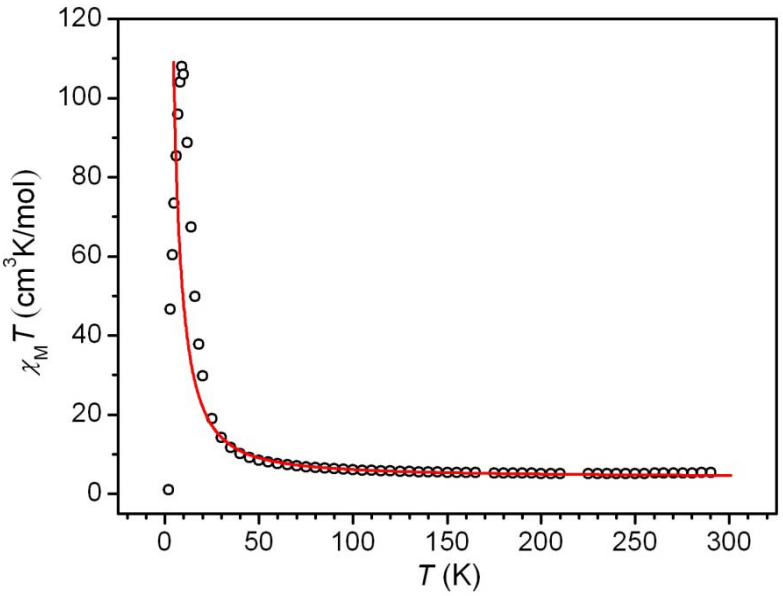

Figure S6. Variable-temperature dc magnetic susceptibility data for **2**, collected in an applied field of 1000 Oe. The solid red line corresponds to a fit to the data, as described in the text.

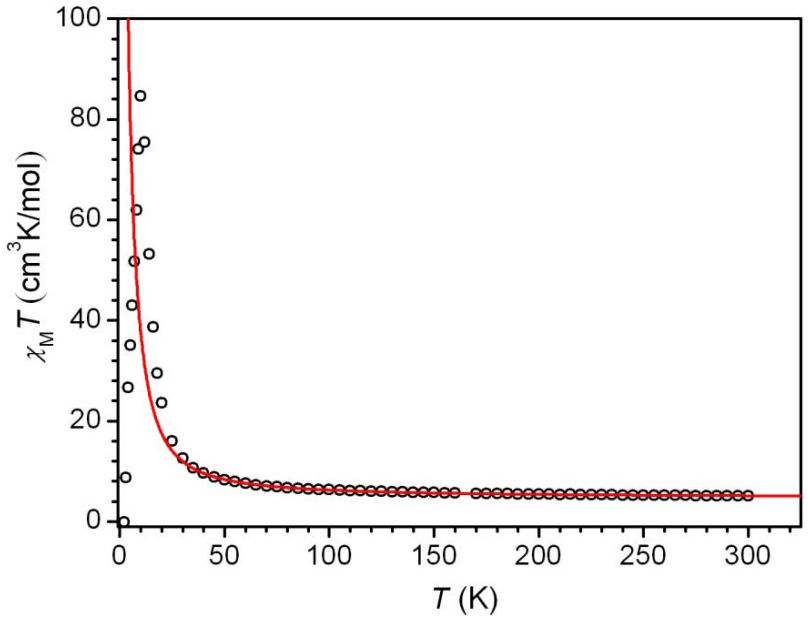

Figure S7. Variable-temperature dc magnetic susceptibility data for **4**, collected in an applied field of 1000 Oe. The solid red line corresponds to a fit to the data, as described in the text.

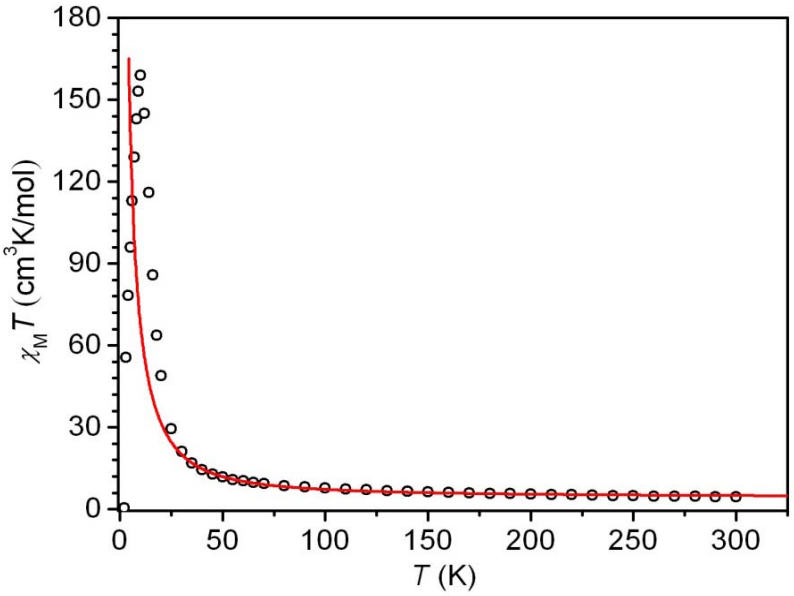

Figure S8. Variable-temperature dc magnetic susceptibility data for **5**, collected in an applied field of 1000 Oe. The solid red line corresponds to a fit to the data, as described in the text.

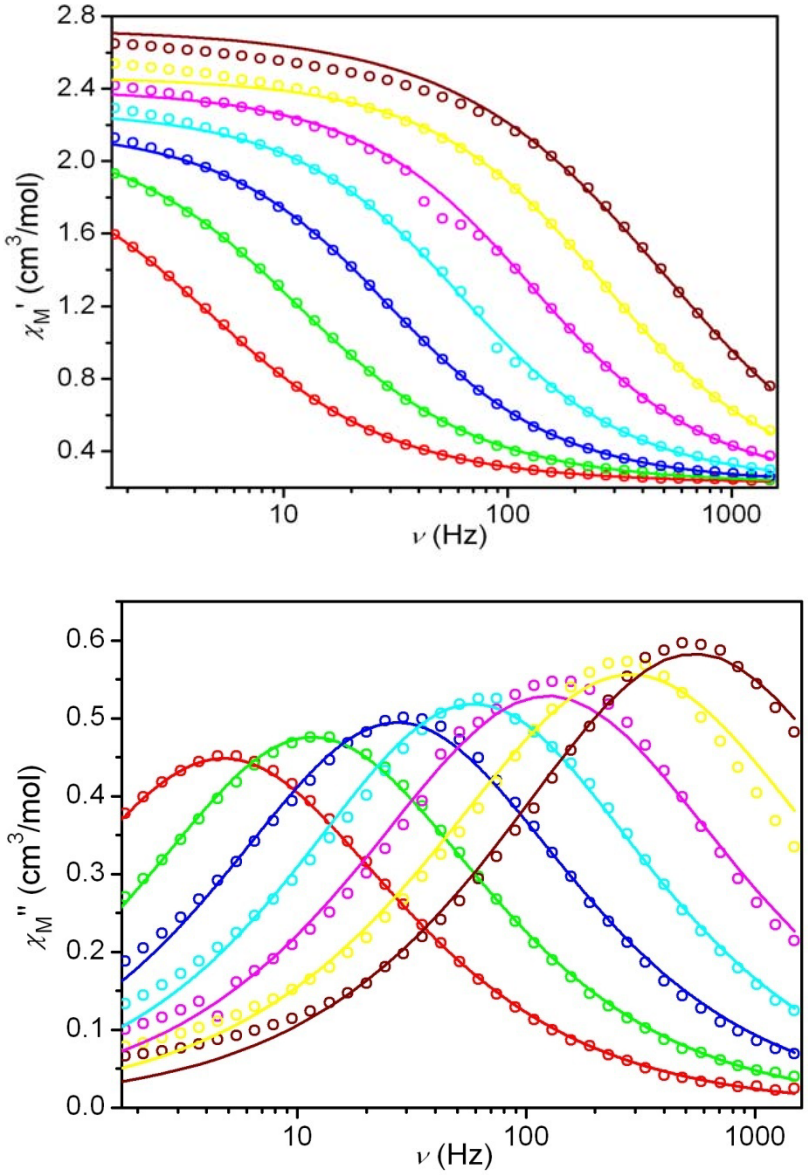

Figure S9. Variable-frequency in-phase (upper) and out-of-phase (lower) components of the ac magnetic susceptibility data for **1**, collected in a 4 Oe ac field at temperatures of 3.6 (red), 3.8 (green), 4.0 (blue), 4.2 (cyan), 4.4 (magenta), 4.6 (yellow) and 4.8 (wine) K. The solid lines correspond to the fits to the data, as described in the text.

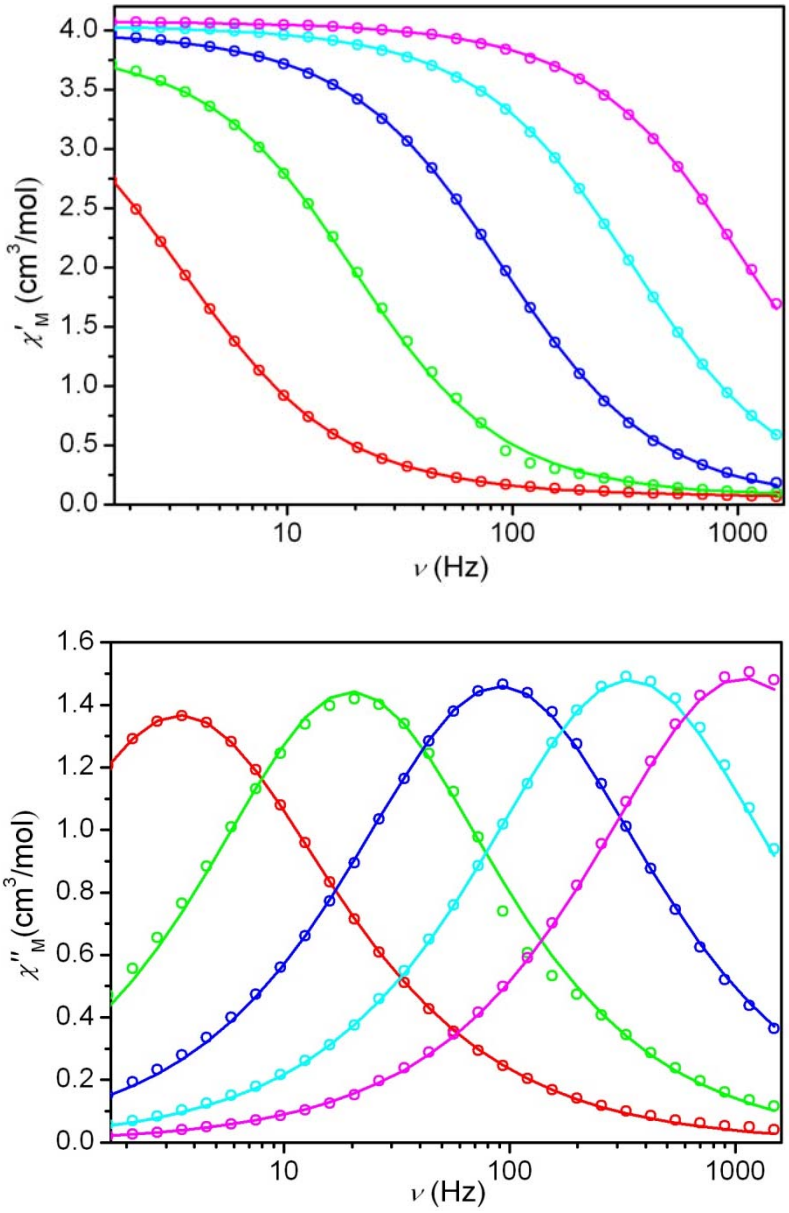

Figure S10. Variable-frequency in-phase (upper) and out-of-phase (lower) components of the ac magnetic susceptibility data for **2**, collected in a 4 Oe ac field at temperatures of 4.0 (red), 4.4 (green), 4.8 (blue) and 5.2 (cyan) and 5.6 (magenta) K. The solid lines correspond to the fits to the data, as described in the text.

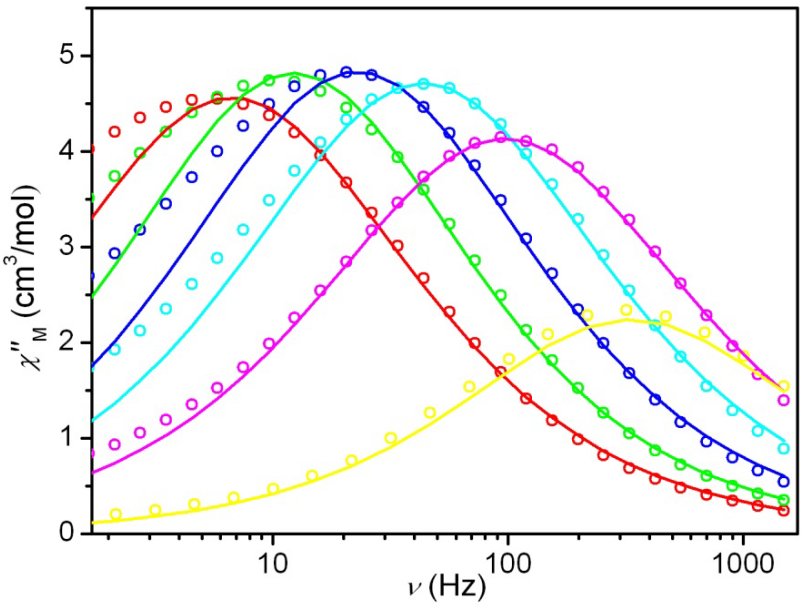

Figure S11. Variable-frequency out-of-phase components of the ac magnetic susceptibility data for **4**, collected under 0 Oe dc field, in a 4 Oe ac field oscillating at temperatures of 9 (red), 9.3 (green), 9.6 (blue), 9.9 (cyan), 10.2 (magenta), and 10.5 (yellow) K. The solid lines correspond to the fits to the data, as described in the text.

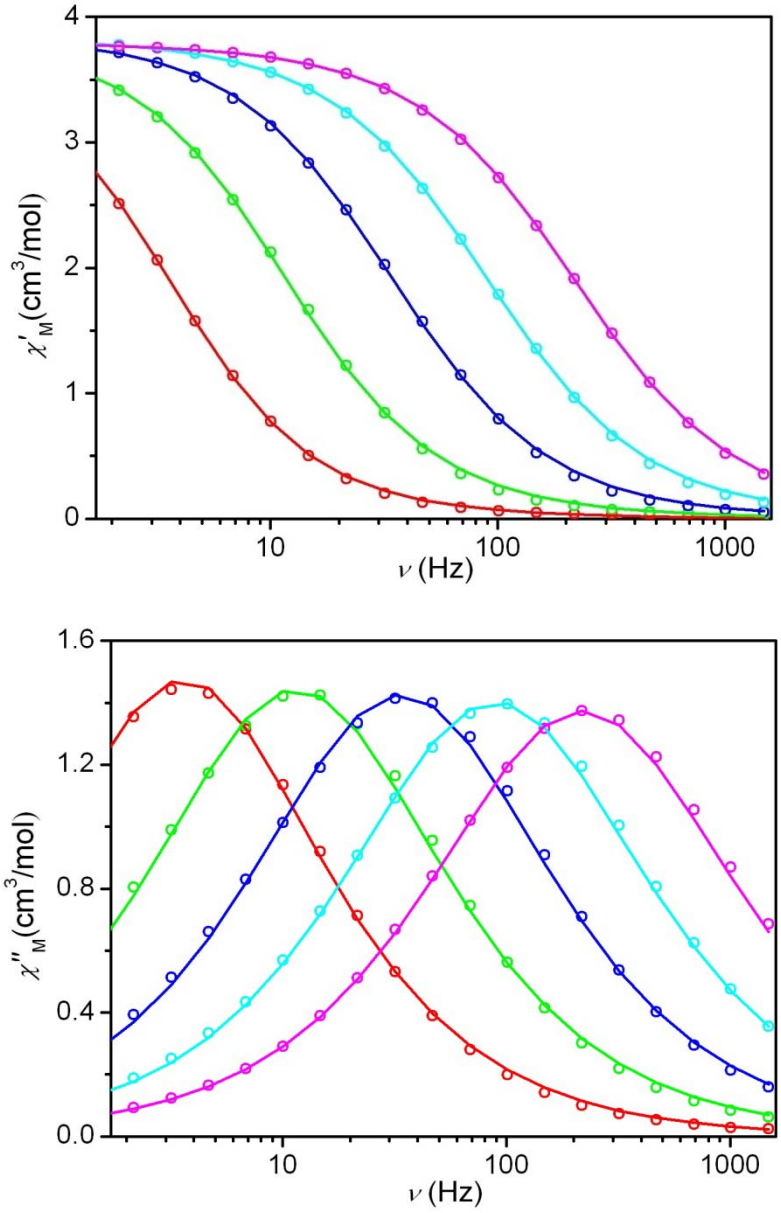

Figure S12. Variable-frequency in-phase (upper) and out-of-phase (lower) components of the ac magnetic susceptibility data for **4**, under a 1000 Oe dc field, collected in a 4 Oe ac field at temperatures of 4 (red), 4.3 (green), 4.6 (blue), 4.9 (cyan) and 5.2 (magenta) K. The solid lines correspond to the fits to the data, as described in the text.

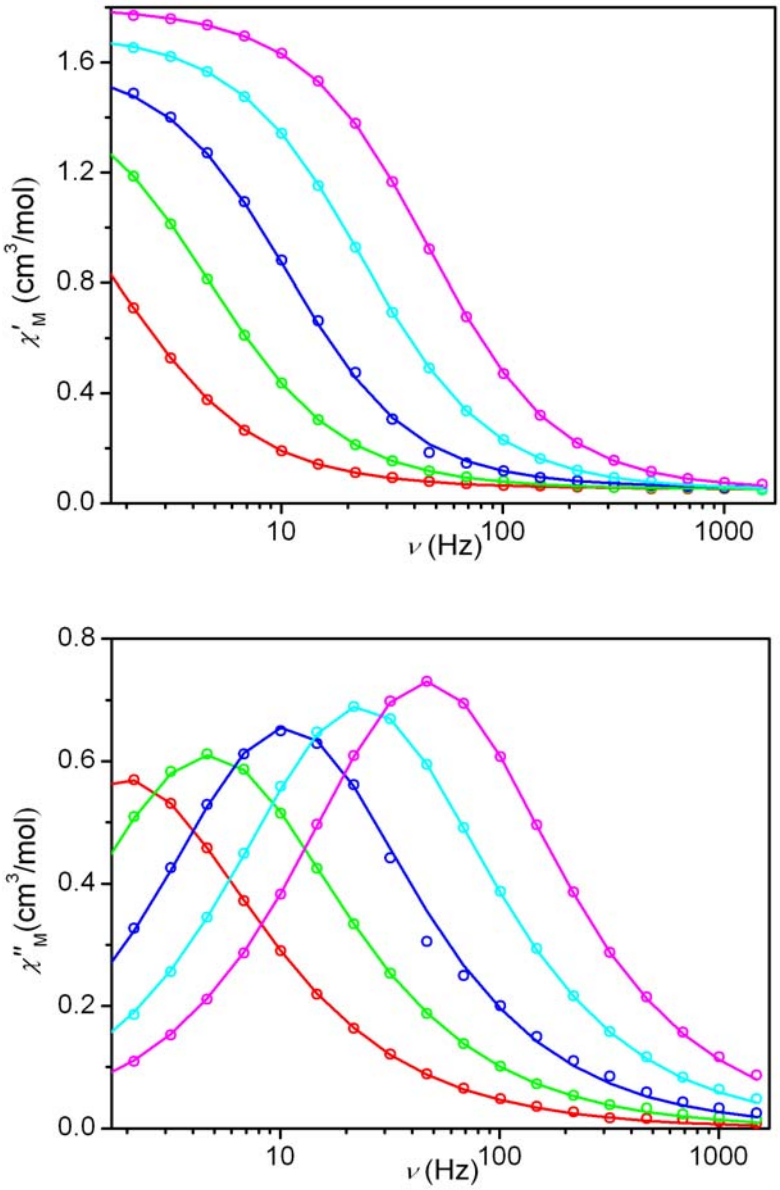

Figure S13. Variable-frequency in-phase (upper) and out-of-phase (lower) components of the ac magnetic susceptibility data for **5**, collected in a 4 Oe ac field at temperatures of 4 (red), 4.2 (green), 4.4 (blue), 4.6 (cyan) and 4.8 (magenta) K. The solid lines correspond to the fits to the data, as described in the text.

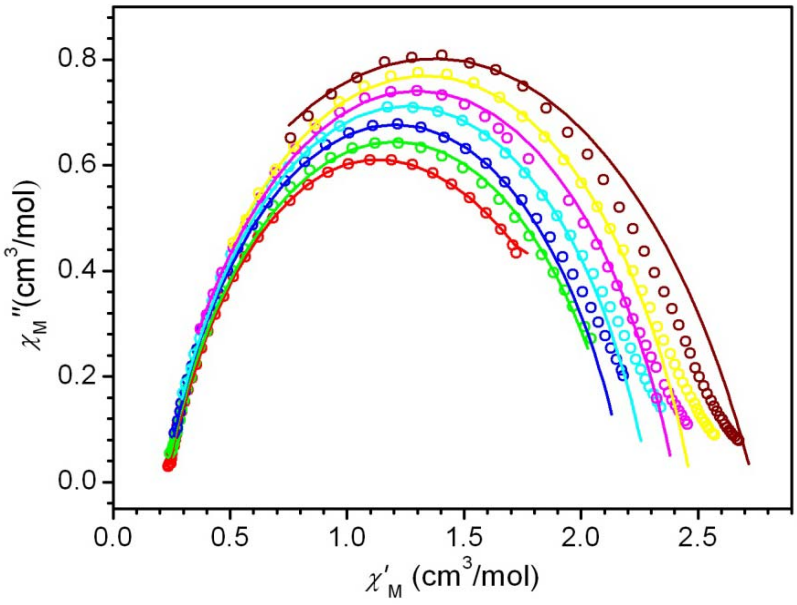

Figure S14. Cole-Cole plots for **1** at temperatures of 3.6 (red), 3.8 (green), 4.0 (blue), 4.2 (cyan), 4.4 (magenta), 4.6 (yellow) and 4.8 (wine) K. The solid lines correspond to the fits to the data, as described in the text.

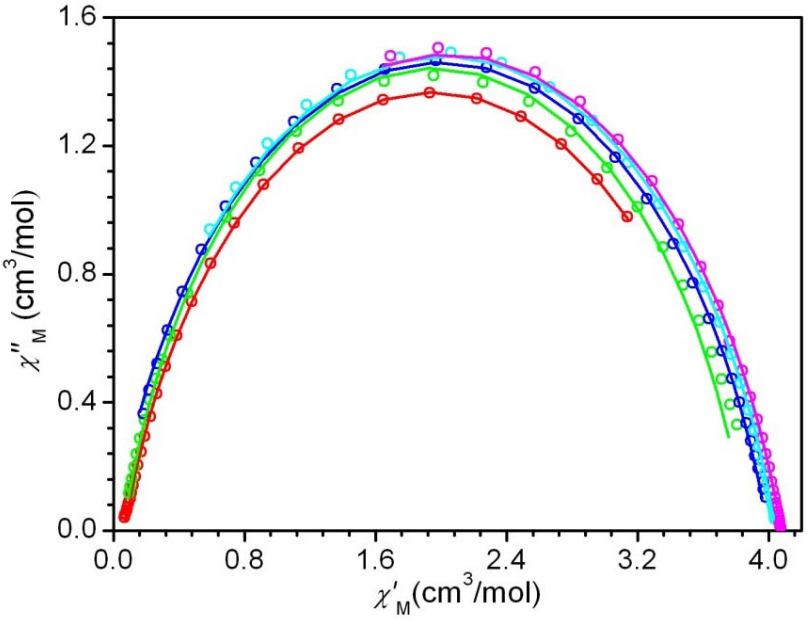

Figure S15. Cole-Cole plots for **2** at temperatures of 4.0 (red), 4.4 (green), 4.8 (blue) and 5.2 (cyan) and 5.6 (magenta) K. The solid lines correspond to the fits to the data, as described in the text.

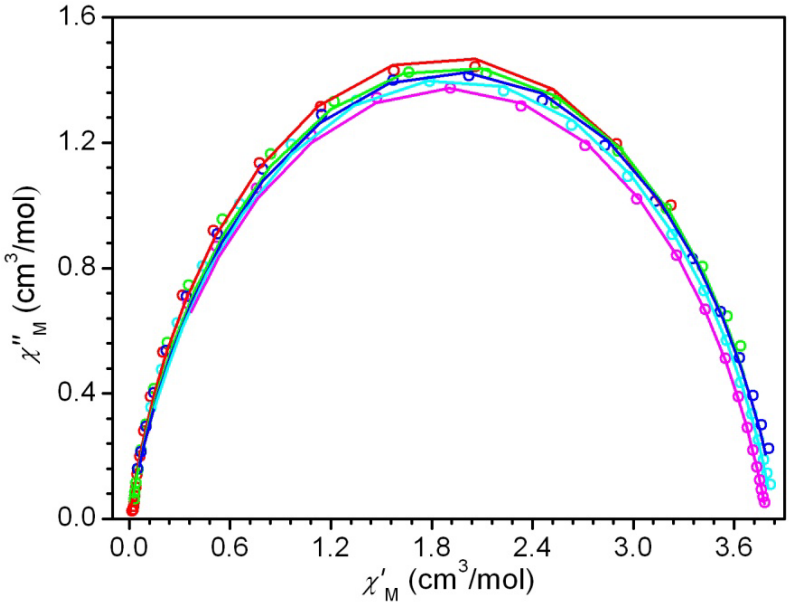

Figure S16. Cole-Cole plots for **4**, constructed from data collected under a 1000 Oe dc field, at temperatures of 4 (red), 4.3 (green), 4.6 (blue), 4.9 (cyan) and 5.2 (magenta) K. The solid lines correspond to the fits to the data, as described in the text.

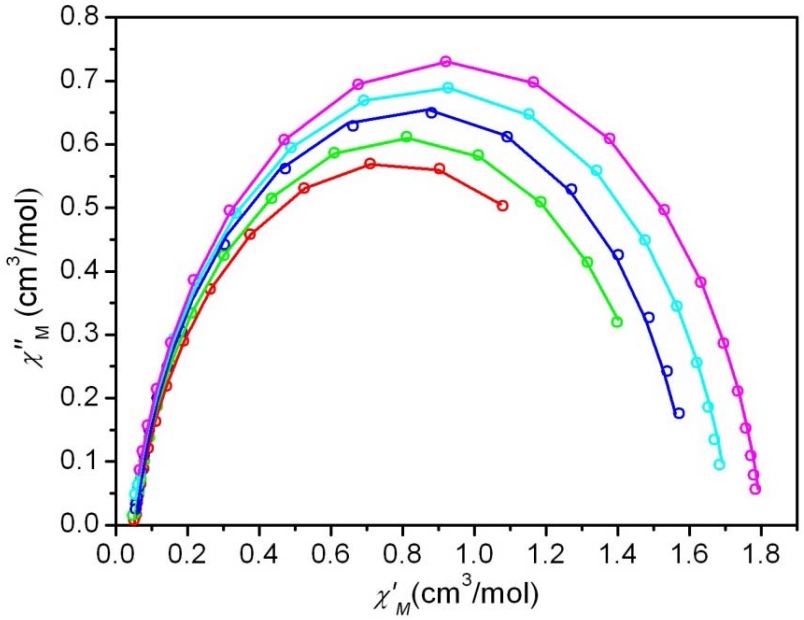

Figure S17. Cole-Cole plots for **5** at temperatures of 4 (red), 4.2 (green), 4.4 (blue), 4.6 (cyan) and 4.8 (magenta) K. The solid lines correspond to the fits to the data, as described in the text.

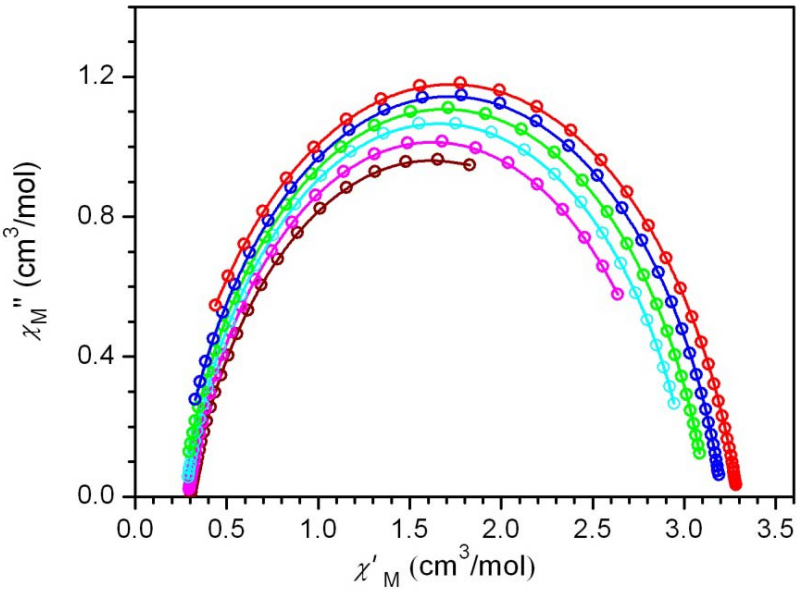

Figure S18. Cole-Cole plots for **6** at temperatures of 6.2 (wine), 6.6 (magenta), 7.0 (cyan), 7.4 (green), 7.8 (blue), and 8.2 (red) K. The solid lines correspond to the fits to the data, as described in the text.

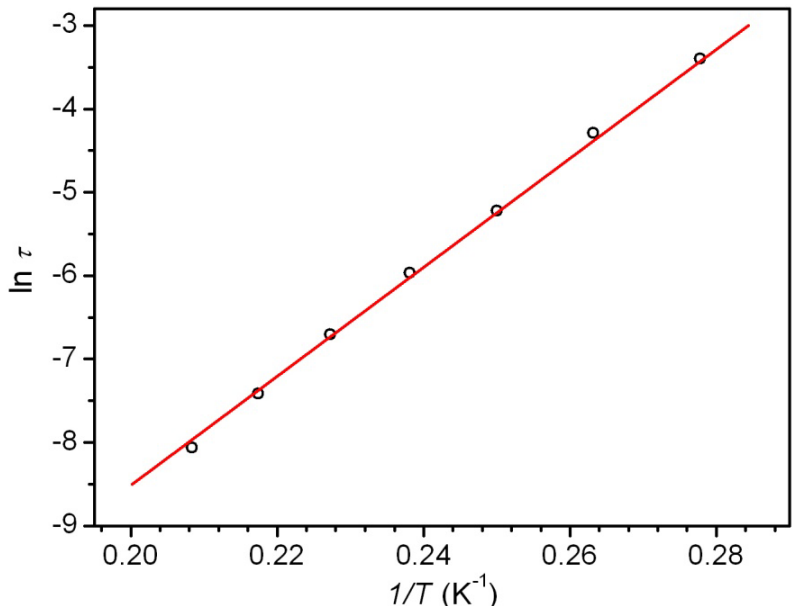

Figure S19. Arrhenius plot of relaxation time for **1**.

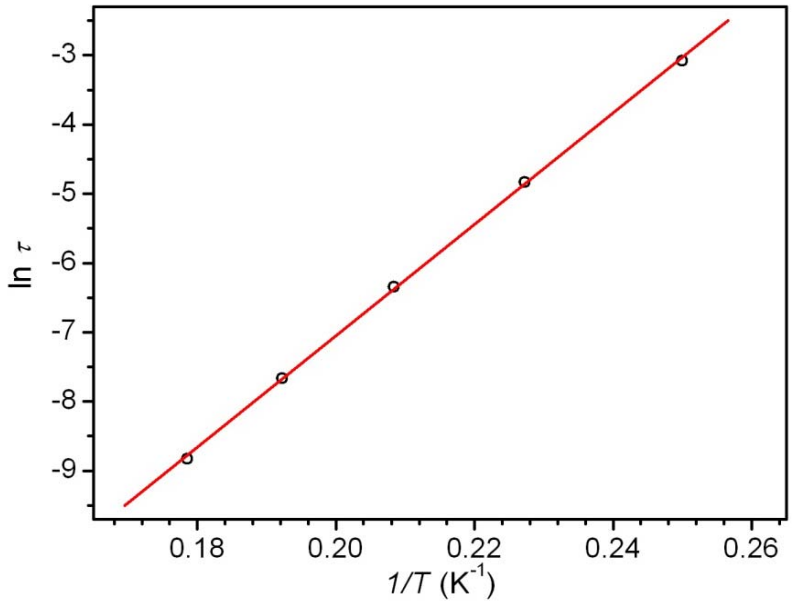

Figure S20. Arrhenius plot of relaxation time for **2**.

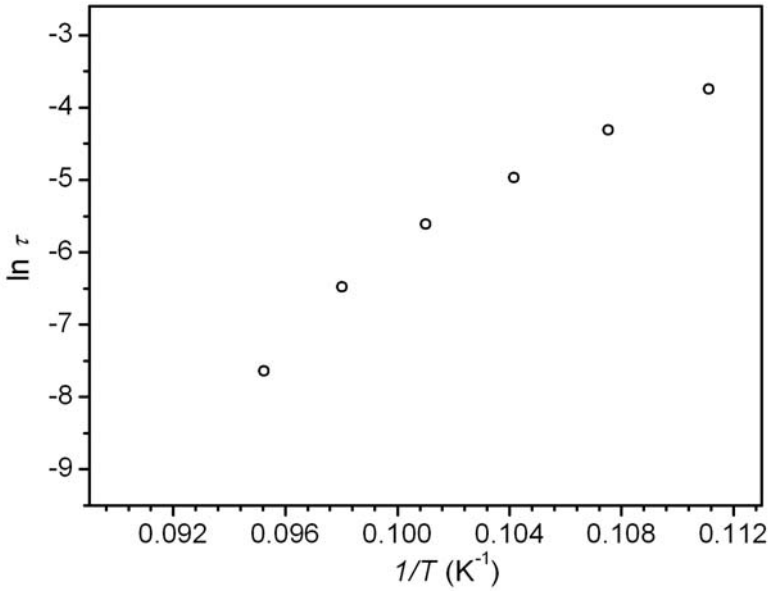

Figure S21. Arrhenius plot of relaxation time for **4**, under a zero dc field.

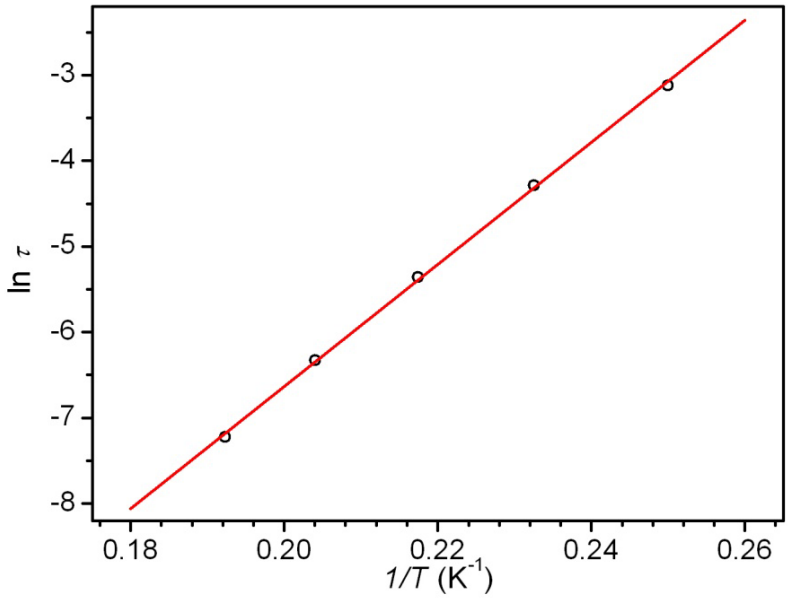

Figure S22. Arrhenius plot of relaxation time for **4**, under a 1000 Oe dc field.

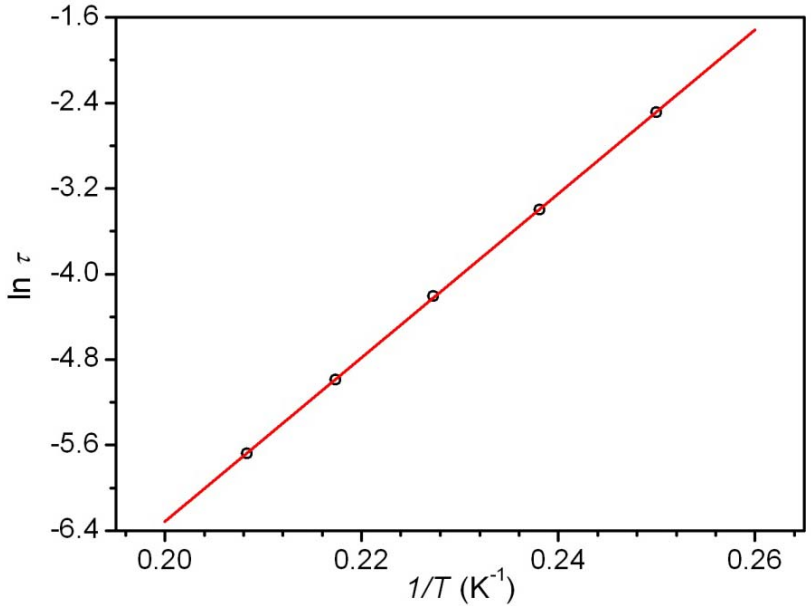

Figure S23. Arrhenius plot of relaxation time for **5**.

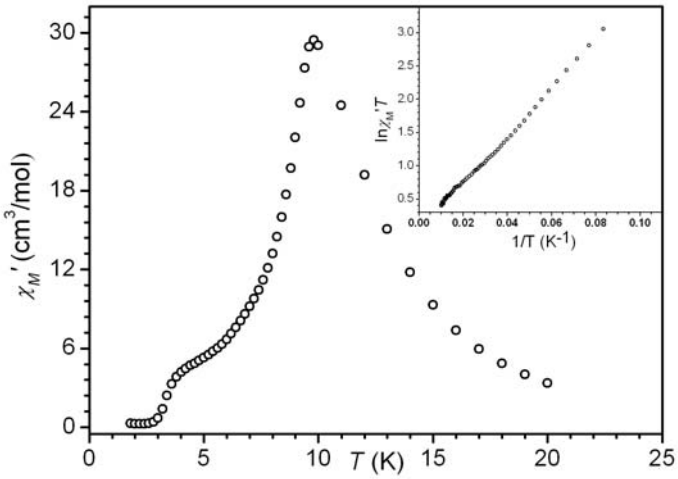

Figure S24. Variable-temperature in-phase component of ac susceptibility of **1**, collected in a 4 Oe ac field oscillating at 1 Hz. Inset: Plot of In($\chi_M'T$) vs $1/T$ for **1**, from 10 K to 100 K

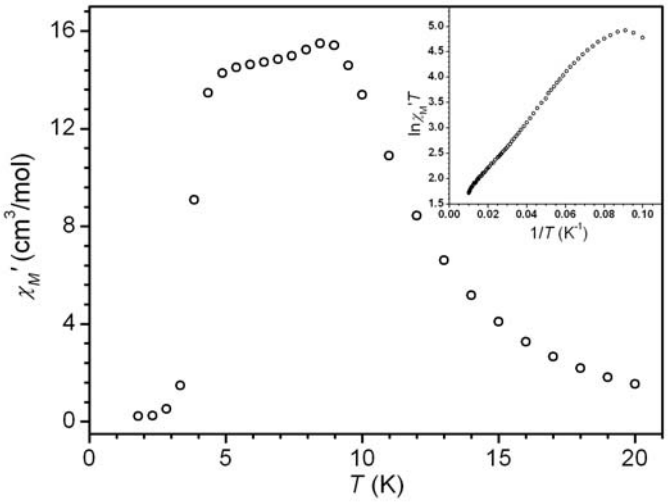

Figure S25. Variable-temperature in-phase component of ac susceptibility of **2**, collected in a 4 Oe ac field oscillating at 1 Hz. Inset: Plot of In($\chi_M'T$) vs $1/T$ for **2**, from 10 K to 100 K

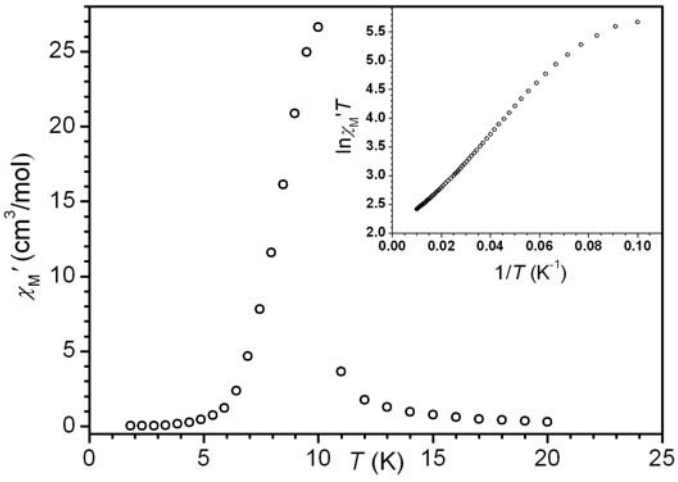

Figure S26. Variable-temperature in-phase component of ac susceptibility of **4**, collected in a 4 Oe ac field oscillating at 1 Hz. Inset: Plot of In($\chi_M'T$) vs 1/T for **4**, from 10 K to 100 K

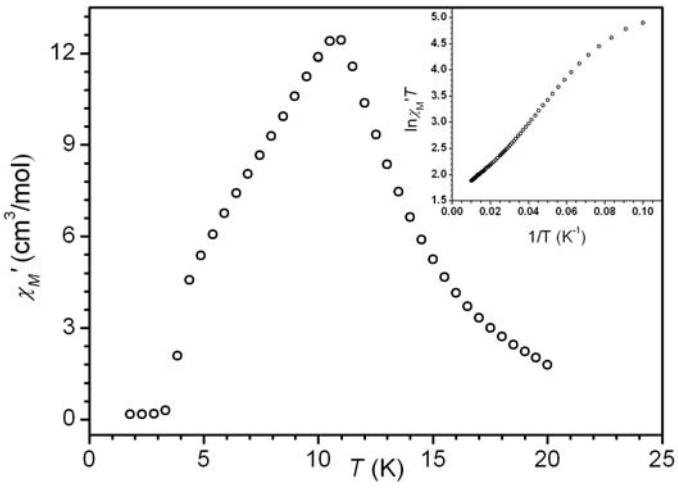

Figure S27. Variable-temperature in-phase component of ac susceptibility of **5**, collected in a 4 Oe ac field oscillating at 1 Hz. Inset: Plot of In($\chi_M'T$) vs 1/T for **5**, from 10 K to 100 K

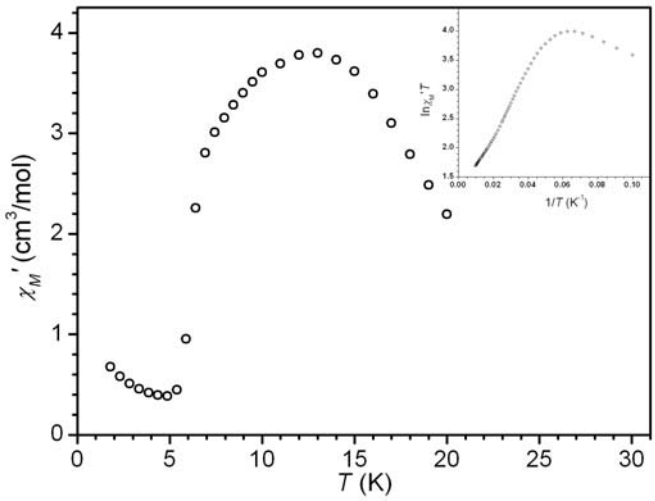

Figure S28. Variable-temperature in-phase component of ac susceptibility of **6**, collected in a 4 Oe ac field oscillating at 1 Hz. Inset: Plot of In($\chi_M'T$) vs 1/T for **6**, from 10 K to 100 K